arXiv:1107.5932v1 [astro-ph.CO] 29 Jul 2011

A Study of Gravitational Lens Chromaticity with the Hubble Space Telescope[1]

J.A. Muñoz[1], E. Mediavilla[2], C.S. Kochanek[3], E.E. Falco[4] and A.M. Mosquera [1,3]

[1]Departamento de Astronomía y Astrofísica, Universidad de Valencia, E-46100 Burjassot, Valencia, Spain

[2]Instituto de Astrofísica de Canarias, E-38200 La Laguna, Tenerife, Spain

[3]Department of Astronomy, The Ohio State University, Columbus, OH 43210, USA

[4]Harvard-Smithsonian Center for Astrophysics, 60 Garden St., Cambridge, MA 02138, USA

email: jmunoz@uv.es

ABSTRACT

We report Hubble Space Telescope observations of 6 gravitational lenses with the Advanced Camera for Surveys. We measured the flux ratios between the lensed images in 6 filters from 8140Å to 2200Å. In 3 of the systems, HE0512−3329, B1600+434, and H1413+117, we were able to construct UV extinction curves partially overlapping the 2175Å feature and characterize the properties of the dust relative to the Galaxy and the Magellanic Clouds. In HE1104−1804 we detect chromatic microlensing and use it to study the physical properties of the quasar accretion disk. For a Gaussian model of the disk $\exp(-r^2/2r_s^2)$, scaling with wavelength as $r_s \propto \lambda^p$, we estimate $r_s(\lambda 3363) = 4^{+4}_{-2}$ (7 ± 4) light-days and $p = 1.1 \pm 0.6$ (1.0 ± 0.6) for a logarithmic (linear) prior on r_s. The remaining two systems, FBQ0951+2635 and SBS1520+530, yielded no useful estimates of extinction or chromatic microlensing.

Subject headings: cosmology: observations — gravitational lensing — dust, extinction, accretion, accretion disk — galaxies: ISM

[1]Based on observations made with the NASA/ESA Hubble Space Telescope. The Space Telescope Science Institute is operated by the Association of Universities for Research in Astronomy, Inc. under NASA contract NAS 5-26555.

1. Introduction

The wavelength-dependent flux ratios between gravitationally lensed images of quasars can be used to probe both the extinction law in the lens galaxy and the unresolved structure of the quasar. Each image is differentially extincted by dust along the path of the image through the lens galaxy, and this can be used to measure the extinction, the extinction law, and the lens redshift (e.g. Nadeau et al. 1991; Falco et al. 1999; Motta et al. 2002; Muñoz et al. 2004; Mediavilla et al. 2005; Eliasdottir et al. 2006, Mosquera et al. 2011). The second effect, microlensing by the stars in the lens galaxy (Chang & Refsdal 1979), leads to wavelength dependent changes in the flux ratios because the effective size of the quasar accretion disk varies with wavelength (Wisotzki et al. 1993, 1995; Wucknitz et al. 2003; Anguita et al. 2008; Bate et al. 2008; Eigenbrod et al. 2008; Poindexter et al.2008; Floyd et al. 2009; Mosquera et al. 2009, 2011; Blackburne et al. 2010; Mediavilla et al. 2011). Detections of "chromaticity" between the images of a lensed quasar are useful for studying both phenomena if they can be disentangled.

In extragalactic astronomy, understanding dust is crucial to understanding galaxies, through its effects on estimates of star formation rates and galaxy evolution (e.g. Conroy et al. 2009), cosmology, through its effects on SNe Ia fluxes (e.g. Jha et al. 2006), and the interpretation of gamma-ray burst afterglows (e.g. Jakobsson et al. 2004)). Unfortunately, classical methods for obtaining accurate extinction curves to characterize dust cannot be used outside the Local Group because they depend on detailed measurements of individual stars. Gravitational lenses are one of the best quantitative astrophysical probes of dust properties at intermediate redshifts given lenses with the right amount of dust and the appropriate combinations of redshifts. If there is too little dust, it is difficult to measure the extinction at long wavelengths and microlensing is more likely to dominate the chromaticity. If there is too much dust, it becomes impossible to measure extinction curves into the rest-frame ultraviolet. Similarly, the lens redshift must be high enough to make the rest-frame 2175Å dust feature observable, while the source redshift must be low enough to avoid having the quasar continuum blocked by absorption in the intergalactic medium. Similar considerations hold for studying chromatic microlensing over the broadest possible wavelength baseline.

We selected six lenses from the survey of extinction by Falco et al. (1999) that roughly satisfied these criteria: HE 0512−3329, FBQ 0951+2635, HE 1104−1805, H 1413+117, SBS 1520+530, and B 1600+434. As we report in §2, we observed them in 6 filters spanning 2200Å to 8100Å (F220W, F250W, F330W, F435W, F555W, F625W and F814W) using the Hubble Space Telescope (HST) and the ACS/HRC camera. This approach ensures that we can measure the image flux ratios without contamination from the lens or the host galaxy

of the quasar. Section 2 also outlines how we model the results to study extinction and microlensing. In §3 we present the results, reporting on the extinction curves of three of the systems and the chromatic microlensing in one system. Section 4 summarizes the results and lessons for future observations.

2. Observations and Analysis

Table 1 provides a log of our ACS/HRC observations based on 13 HST orbits in Cycle 12, Table 2 summarizes previous HST observations of these systems and Table 3 presents our new photometry. The observations in each filter consisted of multiple, dithered sub-exposures which were corrected for cosmic rays and combined using standard methods. We modeled the images following the procedures of Lehár et al. (2000). The images were fit as a combination of point sources, de Vaucouleurs and exponential disk profiles convolved with TinyTim (Krist & Hook 1997) PSF models. We determined the relative astrometry of the components and the structure of the lens galaxy using the CASTLES H-band images where the lens galaxy is best detected and characterized (see Fig. 1). These were then held fixed and the remaining images were fit to determine the fluxes of the components in each filter. For the bluer filters the lens galaxy was undetected and we could easily confirm the model fits with aperture photometry.

Consider multiple images i of a single lensed quasar. Let $m_0(\lambda, t)$ be the intrinsic quasar flux at time t, expressed in magnitudes at observed wavelength λ. The redshifted, extincted flux of image i, is then

$$m_i(\lambda, t) = m_0(\lambda, t) - M_i(\lambda, t) + E_i \; R\left(\frac{\lambda}{1+z_l}\right) \tag{1}$$

where $M_i(\lambda, t)$ and $E_i = E(B-V)$ are the magnification (in magnitudes) and extinction of image i, and $R(\lambda/(1+z_l))$ is the extinction curve at the lens redshift z_l. The magnification $M_i(\lambda, t)$ may depend on wavelength and time due to microlensing effects (Wambsganss 2006 and references therein). By measuring the magnitude differences as a function of wavelength for each image pair (labeled i and j),

$$m_j(\lambda, t) - m_i(\lambda, t) = \Delta M(\lambda, t) + \Delta E \; R\left(\frac{\lambda}{1+z_l}\right) \tag{2}$$

we constrain the relative magnifications, $\Delta M(\lambda, t) = M_j(\lambda, t) - M_i(\lambda, t)$, the extinction differences, $\Delta E(B-V) = E_j(B-V) - E_i(B-V)$, and the mean extinction curve $R(\lambda)$.

For the extinction law $R(\lambda)$ we used either the Cardelli et al. (1989; hereafter CCM) parametrized models for the Galactic extinction curve or the Fitzpatrick & Massa (1990;

hereafter FM) model with its parameters set to match the average extinction in the SMC (Gordon et al. 2003). The main difference is that the Galactic models have a strong 2175Å absorption feature while the SMC models do not. One way to confirm the presence of extinction is to estimate a dust redshift z_d (Jean & Surdej 1998, Falco et al. 1999), the redshift at which the extinction curve best fits the data, and show that it agrees with the observed lens redshift z_l. We assume that the extinction law is the same for all images. Generally one image dominates the extinction and this assumption is unimportant, but it can be an issue if all images are significantly extincted (see Muñoz et al. 2004 and McGough et al. 2005). For models assuming there is only extinction, we fit the data with a single $\Delta M(\lambda, t) \equiv \Delta M$, a common differential magnification for all wavelengths which removes any effects from the magnifications of the macro model and most of the effects of source variability.

The second physical effect in Eqn. 2 is the chromatic microlensing produced by the $\Delta M(\lambda, t)$ term. Because of the structure in the microlensing magnification patterns, the changing size of the disk with wavelength changes the magnification. Since the observer, lens, stars and host galaxy are all in relative motion, this magnification then changes with time. In our present study we will examine this using simulations. Based on the properties of the macro models for the lens geometry, we generate magnification patterns using the approach of Mediavilla et al. (2006), assuming that fraction $\alpha = 0.1$ of the surface density is in stars (i.e. that the surface density is dark matter dominated, see Kochanek et al. 2006, Mediavilla et al. 2009, Pooley et al. 2009, Morgan et al. 2010, Mosquera et al. 2011) and we simply use $M = 1 M_{\odot}$ stars. We then convolve the patterns with Gaussian intensity profiles to model the quasar accretion disk, $I(R) \propto \exp(-R^2/2r_s^2)$ where $r_s \propto \lambda^p$ characterizes the disk size at wavelength λ. These sizes can be rescaled to a different microlensing mass as $\sqrt{M/M_{\odot}}$. We make many random trials fitting the data as a function of r_s and p, and then use Bayesian methods to estimate the size r_s and the scaling exponent p for either linear or logarithmic priors on r_s and linear priors on p, as explained in detail in Mediavilla et al. (2011).

The last point we note is that our data are obtained at a single epoch, so our flux ratios are really comparing $m_0(\lambda, t) - m_0(\lambda, t + \Delta t)$ where Δt is the time delay between the images. This means that intrinsic source variability combined with the time delay between the images can lead to wavelength dependent changes in the flux ratios which we will ignore by assuming that $m_0(\lambda, t) - m_0(\lambda, t + \Delta t) \equiv 0$. Particularly in the estimates of extinction, we will see negligible effects because the parameter ΔM for the difference in the macro model magnifications also captures any achromatic effects from ignoring time variability. For most of the lenses we consider, these changes will be small, as can be seen from the empirical quasar variability models of MacLeod et al. (2010). Yonehara et al.

(2008) based on the ensemble SDSS quasar structure functions (Van den Berk et al. 2004; Ivezic et al. 2004) estimated that there would be typical shifts of ~ 0.1 mag in single epoch observations, but that the changes in colors would be significantly smaller because the color changes associated with quasar variability are far smaller than the overall variability. We can compensate for this problem by using modestly larger uncertainties, but it is really only an issue for systems with long time delays. The worst case is HE 1104−1805 which has a relatively long time delay of almost 6 months. If we follow the procedures of Yonehara et al. (2008), we estimate that the time delay can produce a bias in the shortest wavelength filter (F330W) of roughly 0.1 mag, with a potential color change between the F330W filter and the H-band of only 0.05 mag.

3. Results

We now consider each of the systems individually. We found extinction in HE 0512−3329, B 1600+434 and H 1413+117 and chromatic microlensing in HE 1104−1805. The remaining two systems, FBQ 0951+2635 and SBS 1520+530, did not show enough of a chromaticity signature to perform a deeper analysis given only a single epoch of data. In each of the analyses, it is necessary to determine whether the filters include any broad emission lines, because line and continuum flux ratios can be quite different (e.g. see Mediavilla el al. 2005). While both are equally altered by extinction, the broad emission line regions are more spatially extended and hence far less affected by microlensing (e.g. see Abajas et al. 2002). Here we are restricted to photometry, but by tracking the filter and line locations and widths we can determine the degree of contamination. Fig. 1 shows HST images of the 6 systems. Note that at least half of them are relatively disky, which is not the norm for gravitational lenses.

3.1. HE 0512−3329

HE 0512−3329 is a two image lensed quasar with a separation of $0\farcs65$ and a source redshift of $z_s = 1.565$ (Gregg et al. 2000). The lens redshift is not directly measured, but the presence of a damped Lymanα absorber (DLA) system and associated strong metal line absorption systems suggests that the lens is a spiral galaxy at $z_l = 0.93$ (Gregg et al. 2000, Wucknitz et al. 2003). Table 2 presents the photometry for the lens galaxy as well as the quasar images in the CASTLES data. While the time delays are not measured, they will be so short given the image separation that the single epoch flux ratios will be unaffected by intrinsic variability.

As we see in Fig. 2, the flux ratios have a steep dependence on the wavelength, and the slope is little changed from the earlier CASTLES results or the later results from Eliasdottir et al. (2006). While there are offsets between the epochs indicative of microlensing, they show no significant wavelength dependencies. Wucknitz et al. (2003) show that the broad emission line flux ratios, which should be very little affected by microlensing, show a wavelength dependence consistent with these trends. After correcting for extinction using the broad emission line flux ratios, they also find an effect from microlensing.

Figure 3 shows the result of fitting the flux ratios assuming they are due to differential extinction. Like Wucknitz et al. (2003), and unlike Eliasdottir et al. (2006), we identify a weak 2175Å feature. The Galactic CCM extinction curve fits poorly, with $\chi^2 = 13$ for 4 degrees of freedom (dof), an estimated $R(V) \lesssim 0.5$ and a best fit $R(V) \simeq 0$, a region where the model makes no sense. The model with the weaker feature of the mean SMC extinction law fits far better, with $\chi^2 = 2.8$ for 5 dof and $\Delta E(B-V) = 0.06 \pm 0.01$. If we allow the parameter responsible for the stretch of the bump ($c3$) in the FM extinction law to vary, we find a best fit with $\chi^2 = 1.1$ for 4 dof and parameter $c3 = 1.7 \pm 0.9$ confirming the marginal detection of the bump by Wucknitz et al. (2003). The interpretation of the flux ratios as extinction and the feature as the 2175Å feature seems robust since we obtain a dust redshift of $z_d = 0.92 \pm 0.15$ that is in good agreement with that of the DLA and metal line systems at $z_l = 0.93$ (Gregg et al. 2000, Wucknitz et al. 2003). Although 25% of the CIV emission line lies in the F435W filter, we estimate that differential microlensing between the line and continuum of order 0.2 mag would lead to a line-induced bias in the estimated continuum flux ratios of only ~ 0.01 mag. This is smaller than the photometric uncertainties and cannot explain the observed shift of $\simeq 0.1$ mag.

3.2. B 1600+434

B 1600+434 is a two image system with a separation of $1\farcs4$, a source redshift of $z_s = 1.59$ and a lens redshift of $z_l = 0.41$ (Jackson et al. 1995) where the lens is a nearly edge on spiral (Jaunsen & Hjorth 1997). The time delay is relatively short (~ 47 days, Koopmans et al. 2000, Burud et al. 2000), so single epoch flux ratios will be little affected by intrinsic variability. Not surprisingly, it was quickly found that the image passing through the disk of the galaxy suffered from extinction (Jaunsen & Hjorth 1997, Falco et al. 1999, Burud et al. 2000).

Figure 4 shows the magnitude differences as a function of wavelength, where the redder image A is the image passing through the disk of the lens. The slope of the differences is little changed from the CASTLES observations, but there is an offset of approximately

0.2 mag. Thus, as for HE 0512−3329, the dominant effect is differential extinction with weaker effects due to microlensing that show no obvious wavelength dependence. Figure 5 shows a fit to the flux ratios assuming they are due to extinction, where we have used the 6 cm radio flux ratio (Koopmans et al. 2000) as an extinction-free anchor for the ratios. The data are well fit by a CCM extinction law with $R(V) = 1.5 \pm 0.3$ and $\Delta E(B-V) = 0.39 \pm 0.02$. The structure of the extinction law is not tightly constrained because the 2175Å feature is not only bluewards of our shortest wavelength filter but also lies on top of the Lyα line of the quasar. Dai & Kochanek (2005) estimated a gas column density difference between the images of $\sim 3 \times 10^{21}$ cm^{-2} based on differences in the X-ray spectra of the two images. Using the extinction estimate of $\Delta E(B-V) \simeq 0.1$ from Falco et al. (1999), this implied a dust-to-gas ratio that was somewhat high. However, if we adopt our new estimate, we find a dust-to-gas ratio of $\sim 7 \times 10^{21}$ mag^{-1} cm^{-2} that is very close to the typical Galactic value of 5.8×10^{21} mag^{-1} cm^{-2} (Bohlin et al. 1978).

3.3. H 1413+117

H 1413+117 is a four image system with a maximum separation of $\sim 1\farcs1$ and $z_s = 2.55$ (Magain et al. 1988). The lens galaxy is marginally detected at H-band and its redshift is unknown, although Kneib et al. (1998) propose $z \sim 0.9$ based on the photometric redshifts of nearby galaxies. Figure 6 shows the magnitude differences for our HRC observations, the CASTLES data, the Turnshek (1997) and Chae (2001) data, and the mid-infrared (11μm) flux ratios from MacLeod et al. (2009). The small shifts between the epochs appear to be due to changes in the fluxes of images A and D, at levels of approximately 0.1 and 0.05 mag. The largest wavelength dependencies correspond to images A and B and the lack of significant changes in the colors with time indicates that they should be attributed to extinction. The lack of a wavelength dependence between images D and C suggests they are little affected by either extinction or chromatic microlensing at these wavelengths. The small bump in the F435W magnitude differences including image D (see Fig. 6) is probably due to the contamination by the Lyα emission line. In Figure 6 we also see that the flux ratios excluding image D ($m_A - m_C$, $m_B - m_C$) extend naturally into the mid-IR as might be expected for extinction, while the flux rations including image D ($m_B - m_D$, $m_D - m_C$) show significant shifts (~ 0.2 mag) going from near-IR to the mid-IR. This seems more easily explained by microlensing, where the near-IR emission is from the accretion disk while the mid-IR emission is from thermal dust emission on larger scales.

We conclude that A and B images are significantly affected by differential extinction from the lens galaxy. Unfortunately the lack of a candidate for the 2175 Å feature combined

with the unknown redshift of the lens galaxy makes it difficult to analyze the extinction. If the bump feature is present in the lens galaxy, its absence in our observations implies a very low lens redshift ($\lesssim 0.3$), as illustrated by the example for a lens at $z_l = 0.25$ shown in Fig. 7. The failure to detect the lens in the V and I-band HST observations almost certainly guarantees that the lens redshift cannot be so low. Thus we must conclude that the extinction law in this lens lacks a significant 2175Å feature.

3.4. HE 1104−1805

HE 1104−1805 is a two image lensed quasar with a relatively large separation of $\sim 3\farcs2$ and a source redshift of $z_s = 2.32$ (Wisotzki et al. 1993) and a lens redshift of $z_l = 0.73$ (Lidman et al. 2000). Lehár et al. (2000) modeled the system in detail using the CASTLES images. The time delay is relatively long (~ 162 days, Morgan et al. 2008), but based on the statistics of quasar variability discussed in §2 our single epoch flux ratios should not be strongly biased. Falco et al. (1999) modeled the flux ratios as extinction, although the X-ray absorption study by Dai et al. (2006) found negligible differential absorption. In fact, it was also clear from the later light curves (Schechter et al. 2003, Poindexter et al. 2007) that there was significant chromatic microlensing in this system. Indeed, as Poindexter et al. (2008) noted in their detailed study of microlensing the relative colors of the two images reversed over the period from its discovery, very different from the limited color changes seen in the first three lenses we considered. Further evidence against significant extinction is that the mid-IR flux ratios from Poindexter et al. (2007) agree well with the emission line flux ratios (Wisotzki et al. 1993). Figure 8 shows the magnitude differences for images A and B for each ACS/HRC filter, along with the CASTLES magnitude differences and the mid-IR flux ratios from Poindexter et al. (2007). We can see again the change in slope of the wavelength dependence between the two epochs indicating the detection of chromatic microlensing.

We separately modeled the two epochs of HST observations using the procedures from Mediavilla et al. (2011) and Mosquera et al. (2011), as briefly outlined in §2, to compare the results from single epoch models to the more complex light curve modeling procedures used by Poindexter et al. (2008). Figure 9 shows the estimates for the scale radius r_s in the F336W filter (1013Å in the rest frame) and the logarithmic slope p of the size with wavelength, $r_s \propto \lambda^p$, for the HRC data, the CASTLES data and the combination of the two assuming either a logarithmic or a linear prior on r_s. In thin disk theory, where the disk temperature profile is $T \propto R^{-3/4}$, we would expect to find $p = 4/3$. Given the nature of the chromatic microlensing detected in the HRC observations the uncertainties

are substantially greater than the ones derived from the CASTLES data, with its steeper, monotonic variations in the flux ratios, but the estimates (see Table 4) agree within the uncertainties. When we combine the two results, we find $p = 1.1 \pm 0.6$ and $r_s = 4^{+4}_{-2}$ light-days for the logarithmic prior on the size, and $p = 1.0 \pm 0.6$ and $r_s = 7 \pm 4$ light-days for the linear prior. We can compare to Poindexter et al. (2008), who used a different disk model and normalizing wavelength, by converting the scale lengths to the half-light radii $R_{1/2}$ of the models since Mortonson et al. (2005) showed that different microlensing models will agree on the half-light radius of the distribution. We transform our r_s at $\lambda = 3363$Å to $R_{1/2}(\lambda 4311) = 1.18\ (4311/3363)^p\ r_s(\lambda 3363)$ at the normalizing wavelength $\lambda = 4311$Å used by Poindexter et al. (2008), where their radius r_{disk} corresponds to a half-light radius of $R_{1/2} = 2.49 r_\lambda 4311$. In addition we rescale our microlens mass to $M = 0.3 M_\odot$ from $M = 1 M_\odot$ ($r_s \propto \sqrt{M}$) as this is closer to the expectation for normal stellar populations (see Poindexter et al. 2008). Figure 10 shows that our combined results are in excellent agreement with those of Poindexter et al. (2008).

3.5. FBQ 0951+2635

FBQ 0951+2635 is a two image lens with an image separation of $1\farcs1$, a source redshift of $z_s = 1.24$ (Schechter et al. 1998), and a lens redshift of $z_l = 0.260 \pm 0.002$ (Eigenbrod et al. 2007). The time delay is short, ~ 16 days (Jakobsson et al. 2005) and several studies have detected microlensing variability at the level of 0.04 mag/year (e.g., Schechter et al. 1998, Jakobsson et al. 2005, Paraficz et al. 2006). Figure 11 shows our measurements of the magnitude differences between the two images along with the differences found by CASTLES. The magnitudes of the differences are smaller than in the previous four systems, and it is clear that there is little differential extinction. This agrees with the similar conclusion of Mosquera et al. (2011) based on ground-based narrow band imaging. The UV data from HST allow to us cover the wavelength range where the bump feature is expected given the measured redshift of the lens galaxy. Although we see a small feature in the F250W filter, we cannot simply attribute it to the 2175Å bump because it also overlaps the Lyα emission line of the quasar. The differences between the present data and the CASTLES observations indicate the presence of chromatic microlensing, but the amplitudes are too small for single epoch microlensing models to yield significant results. Nonetheless, we confirm that FBQ 0951+2635 is a good candidate for future measurements, reinforced by the fact that Morgan et al. (2010) were already able to estimate a disk size based on microlensing in the R-band light curves of this source.

3.6. SBS 1520+530

SBS 1520+530 is a two image lens with an image separation of $\simeq 1\farcs6$, a source redshift of $z_s = 1.86$ and a lens redshift of $z_l = 0.72$ (Chavushyan et al. 1997). Burud et al. (2002) measured a time delay for the system of ~ 130 days, and Gaynullina et al. (2005) and Paraficz et al. (2006) observed microlensing at a level of ~ 0.14 mag over roughly 4 years. Morgan et al. (2010) estimated an R-band half-light radius for the disk based on modeling these light curves. Unfortunately our HRC observations do not show a significant chromaticity signal to allow us to perform a deeper analysis. Figure 12 shows the magnitude differences as a function of wavelength for our HRC data and the CASTLES differences presented in Table 2. The wavelength dependent trends in the ACS/HRC observations are weak, indicating that the differential extinction is very low. Interpreting the CASTLES data is difficult because the V-band (F555W) flux ratio is so oddly different. We have inspected the CASTLES data several times and have been unable to find a systematic problem (e.g. missed cosmic rays) that would explain the discrepancies.

4. Discussion and Summary

The effects of both extinction and microlensing become larger as we observe them at shorter wavelengths. Unfortunately, the atmosphere prevents us from observing into the ultraviolet from the ground, and so we generally cannot observe the rest-frame 2175Å region to search for the characteristic feature of Galactic and LMC extinction curves or to probe the hot regions near the inner edges of accretion disks. Here we surveyed six gravitational lenses with evidence for significant wavelength dependent flux ratios in the extinction study of Falco et al. (1999) from the I-band into the UV (8100Å to 2200Å). Two of the lenses, FBQ 0951+2635 and SBS 1520+530, showed changes with wavelength that were too small to yield interesting constraints.

It is not surprising given the selection method that three of the lenses show significant evidence for differential extinction between the images. We argue for extinction dominating over chromatic microlensing systems based on the lack of evidence for significant time variability in the color, although all three systems show small changes in the flux ratios that are probably due to microlensing. In the case of HE 0512−3329 we find evidence for a weak 2175Å feature from the dust in the $z_l = 0.93$ lens. For B 1600+434 we cannot quite reach the wavelengths needed to quantify the presence of the 2175Å feature, although a CCM extinction law agrees with our observations, while the lack of a lens redshift for H 1413+117 limits our conclusions. Both systems contain significant differential extinction, and it is likely that the dust in B 1600+434 has the 2175Å feature and that the dust in H 1413+177

does not.

We clearly detect chromatic microlensing in HE 1104−1805. If we estimate the wavelength dependent size of the accretion disk by modeling our single epoch of data or the earlier CASTLES data, we find compatible results. If we combine the two single epoch estimates, the combined result agrees with the multi-band light curve analyses of Poindexter et al. (2008). Modeled as a Gaussian source $\exp(-r^2/2r_s^2)$ with $r_s \propto \lambda^p$ and normalized at the observed wavelength $\lambda = 3363$ Å we find $r_s = 4^{+4}_{-2}$ (7 ± 4) and $p = 1.1 \pm 0.6$ (1.0 ± 0.6) for a logarithmic (linear) prior on r_s. These slopes are consistent with the expected slopes from standard thin disk theory ($T \propto R^{-1/p}$ with p=4/3), but the uncertainties are too large to draw a stronger conclusion.

This research was supported by the European Community's Sixth Framework Marie Curie Research Training Network Programme, Contract No. MRTN-CT-2004-505183 "ANGLES", and by the Spanish Ministerio de Educación y Ciencias (grants AYA2007-67342-C03-01/03 and AYA2010-21741-C03/02). J.A.M. is also supported by the Generalitat Valenciana with the grant PROMETEO/2009/64. A.M.M. is also supported by Generalitat Valenciana, grant APOSTD/2010/030. CSK is supported in part by NSF grant AST-1009756. Based on observations made with the NASA/ESA Hubble Space Telescope, obtained at the Space Telescope Science Institute, which is operated by the Association of Universities for Research in Astronomy, Inc., under NASA contract NAS 5-26555. These observations are associated with program GO-9896.

REFERENCES

Abajas, C., Mediavilla, E., Muñoz, J. A., Popović, L. C., & Oscoz, A. 2002, ApJ, 576, 640

Anguita, T., Schmidt, R. W., Turner, E. L., Wambsganss, J., Webster, R. L., Loomis, K. A., Long, D., & McMillan, R. 2008, A&A, 480, 327

Bate, N. F., Floyd, D. J. E., Webster, R. L., & Wyithe, J. S. B. 2008, MNRAS, 391, 1955

Blackburne, J. A., & Kochanek, C. S. 2010, ApJ, 718, 1079

Bohlin, R. C., Savage, B. D., & Drake, J. F. 1978, ApJ, 224, 132

Burud, I., et al. 2000, ApJ, 544, 117

Burud, I., et al. 2002, A&A, 391, 481

Cardelli, J.A., Clayton, G.C. & Mathis, J.S., 1989, ApJ, 345, 245

Chae, K.-H., Turnshek, D. A., Schulte-Ladbeck, R. E., Rao, S. M., & Lupie, O. L. 2001, ApJ, 561, 653

Chang, K., & Refsdal, S. 1979, Nature, 282, 561

Chavushyan, V. H., Vlasyuk, V. V., Stepanian, J. A., & Erastova, L. K. 1997, A&A, 318, L67

Conroy, C., Gunn, J. E., & White, M. 2009, ApJ, 699, 486

Dai, X., & Kochanek, C. S. 2005, ApJ, 625, 633

Dai, X., Kochanek, C. S., Chartas, G., & Mathur, S. 2006, ApJ, 637, 53

Eigenbrod, A., Courbin, F., & Meylan, G. 2007, A&A, 465, 51

Eigenbrod, A., Courbin, F., Meylan, G., Agol, E., Anguita, T., Schmidt, R. W., & Wambsganss, J. 2008, A&A, 490, 933

Eliasdottir, A., Hjorth, J., Toft, S., Burud, I., & Paraficz, D. 2006, ApJS, 166, 443

Falco, E. E. et al. 1999, ApJ, 523, 617

Fitzpatrick, E.L,. & Massa, D., 1988, ApJ, 307, 734

Floyd, D. J. E., Bate, N. F., & Webster, R. L. 2009, MNRAS, 398, 233

Gaynullina, E. R., Schmidt, R. W., Akhunov, T., Burkhonov, O., Gottlober, S., Mirtadjieva, K., Nuritdinov, S. N., Tadjibaev, I., Wambsganss, J., & Wisotzki, L. 2005, A&A, 440, 53

Gordon, K. D., Clayton, G. C., Misselt, K. A., Landolt, A. U., & Wolff, M. J. 2003, ApJ, 594, 279

Gregg, M. D.,Wisotzki, L., Becker, R.H., Maza, J., Schechter, P. L., White,R. L., Brotherton, M. S., & Winn, J. N. 2000, AJ, 119, 2535

Ivezic, Ž., et al. 2004, The Interplay Among Black Holes, Stars and ISM in Galactic Nuclei, 222, 525

Jakobsson, P., et al. 2004, A&A, 427, 785

Jakobsson, P., Hjorth, J., Burud, I., Letawe, G., Lidman, C. & Courbin, F. 2005, A&A, 431, 103

Jackson, N., et al. 1995, MNRAS, 274, L25

Jaunsen, A. O. & Hjorth, J. 1997, A&A, 317, L39

Jean, C. & Surdej, J. 1998, A&A, 339, 729

Jha, S., et al. 2006, AJ, 131, 527

Kneib, J.-P., Alloin, D., & Pello, R. 1998, A&A, 339, L65

Kochanek, C. S., Morgan, N. D., Falco, E. E., McLeod, B. A., Winn, J. N., Dembicky, J., & Ketzeback, B. 2006, ApJ, 640, 47

Koopmans, L. V. E., de Bruyn, A. G., Xanthopoulos, E., & Fassnacht, C. D. 2000, A&A, 356, 391

Krist, J. E., & Hook, R. N. 1997, The 1997 HST Calibration Workshop with a New Generation of Instruments , 192

Lehár, J., et al. 2000, ApJ, 536, 584

Lidman, C., Courbin, F., Kneib, J.-P., Golse, G., Castander, F., & Soucail, G. 2000, A&A, 364, L62

McGough, C., Glayton, G. C., Gordon, K. D., & Wolff, M. J. 2005, ApJ, 624, 118

MacLeod, C. L., Kochanek, C. S., & Agol, E. 2009, ApJ, 699, 1578

MacLeod, C. L., et al. 2010, ApJ, 721, 1014

Magain, P., Surdej, J., Swings, J.-P., Borgeest, U., Kayser, R., Kühr, H., Refsdal, S., & Remy, M. 1988, Nature, 334, 325

Mediavilla, E., Muñoz, J. A., Kochanek, C. S., Falco, E. E., Arribas, S., & Motta, V. 2005, ApJ, 619, 749

Mediavilla, E., Muñoz, J. A., Lopez, P., et al. 2006, ApJ, 653, 942

Mediavilla, E., Muñoz, J. A., Falco, E. E. et al. 2009, ApJ, 706, 1451

Mediavilla, E., Muñoz, J. A., Kochanek C. S. et al. 2011, ApJ, 730, 16

Morgan, C. W., Kochanek, C. S., Dai, X., Morgan, N. D., & Falco, E. E. 2008, ApJ, 689, 755

Morgan, C. W., Kochanek, C. S., Morgan, N. D., & Falco, E. E. 2010, ApJ, 712, 1129

Mortonson, M. J., Schechter, P. L., & Wambsganss, J. 2005, ApJ, 628, 594

Mosquera, A. M., Muñoz, J. A., & Mediavilla, E. 2009, ApJ, 691, 1292

Mosquera, A. M., Muñoz, J. A., Mediavilla, E., & Kochanek C. S. 2011, ApJ, 728, 145

Motta, V., Mediavilla, E., Muñoz, J.A. et al. 2002, ApJ, 574, 719

Muñoz, J. A., Falco, E. E., Kochanek, C. S., McLeod, B. A., & Mediavilla, E. 2004, ApJ, 605, 614

Nadeau, D., Yee, H. K. C., Forrest, W. J., Garnett, J. D., Ninkov, Z., & Pipher, J. L. 1991, ApJ, 376, 430

Paraficz, D., Hjorth, J., Burud, I., Jakobsson, P., & Eliasdottir, A., 2006, A&A, 455, 1

Poindexter, S., Morgan, N., Kochanek, C. S., & Falco, E. E. 2007, ApJ, 660, 146

Poindexter, S., Morgan, N., & Kochanek, C. S. 2008, ApJ, 673, 34

Pooley, D., Rappaport, S., Blackburne, J., Schechter, P. L., Schwab, J., & Wambsganss, J. 2009, ApJ, 697, 1892

Schechter, P. L., Gregg, M. D., Becker, R. H., Helfand, D. J., & White, R. L. 1998, AJ, 115, 1371

Schechter, P. L., et al. 2003, ApJ, 584, 657

Turnshek, D. A., Lupie, O. L., Rao, S. M., Espey, B. R., & Sirola, C. J. 1997, ApJ, 485, 100

Vanden Berk, D. E., et al. 2004, ApJ, 601, 692

Wambsganss, J. 2006, in Saas-Fee Advanced Course 33, Gravitational Lensing: Strong, Weak and Micro, ed. G. Meylan, P. Jetzer, & P. North (Berlin: Spri nger), 453

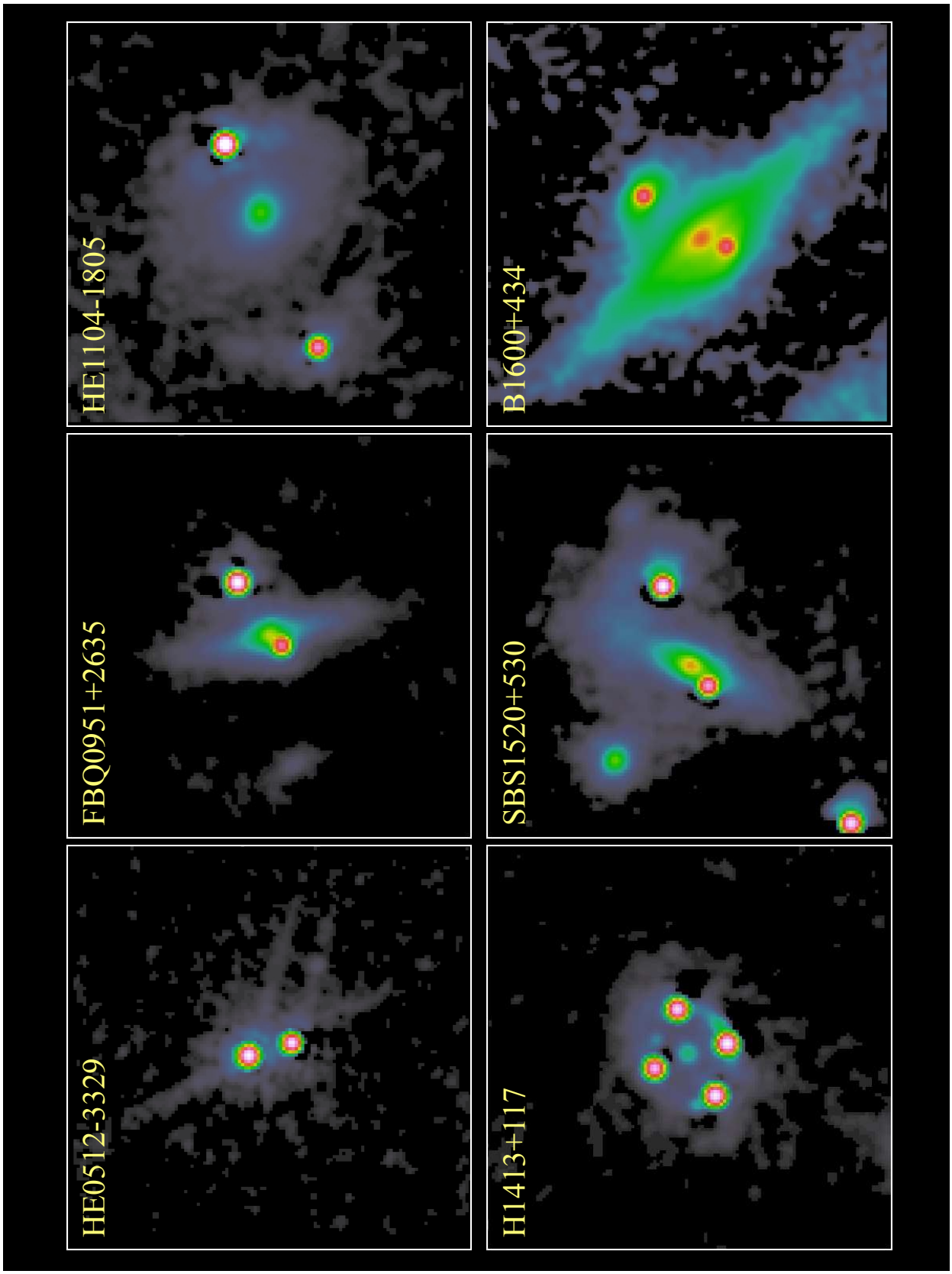
Wisotzki, L., Köhler, T., Kayser, R., & Reimers, D. 1993, A&A, 278, L15

Wisotzki, L., Koehler, T., Ikonomou, M., & Reimers, D. 1995, A&A, 297, 59

Wucknitz, O., Wisotzki, L., Lopez, S., & Gregg, M. D. 2003, A&A, 405, 445

Yonehara, A., Hirashita, H., & Richter, P. 2008, A&A, 478, 95

This preprint was prepared with the AAS LaTeX macros v4.0.


HE0512-3329
FBQ0951+2635
HE1104-1805
H1413+117
SBS1520+530
B1600+434

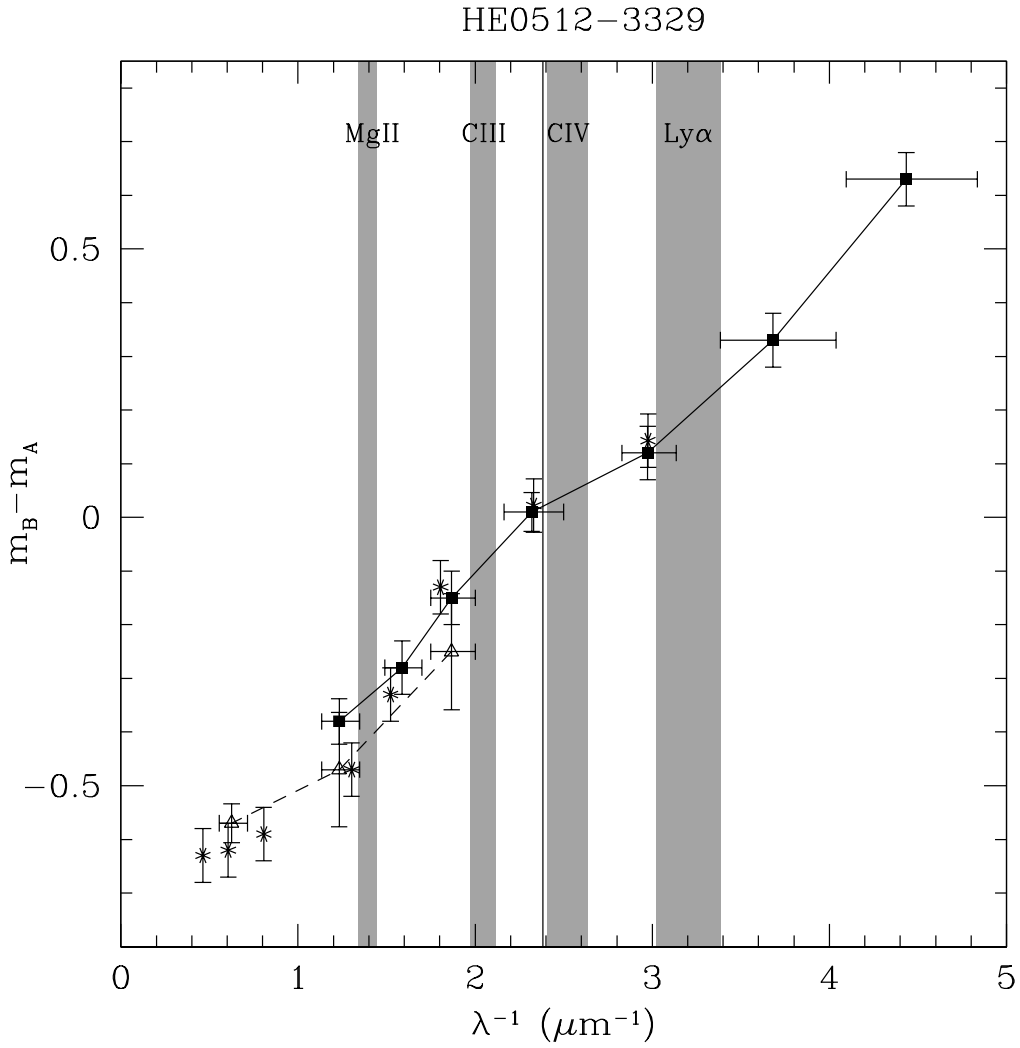


Fig. 2.— Magnitude differences of HE 0512−3329 as a function of the inverse of the observed wavelength for the new HST observations (filled squares) along with the previous CASTLES observations (open triangles) and the ground-based data from Eliasdottir et al. (2006) (asterisks). The shaded regions correspond to the wavelength location and width of the most prominent quasar broad emission lines. The vertical solid line indicates the expected position of the 2175Å extinction curve feature based on the estimated lens redshift. The horizontal error bars on the HST data indicate the widths of the filters.

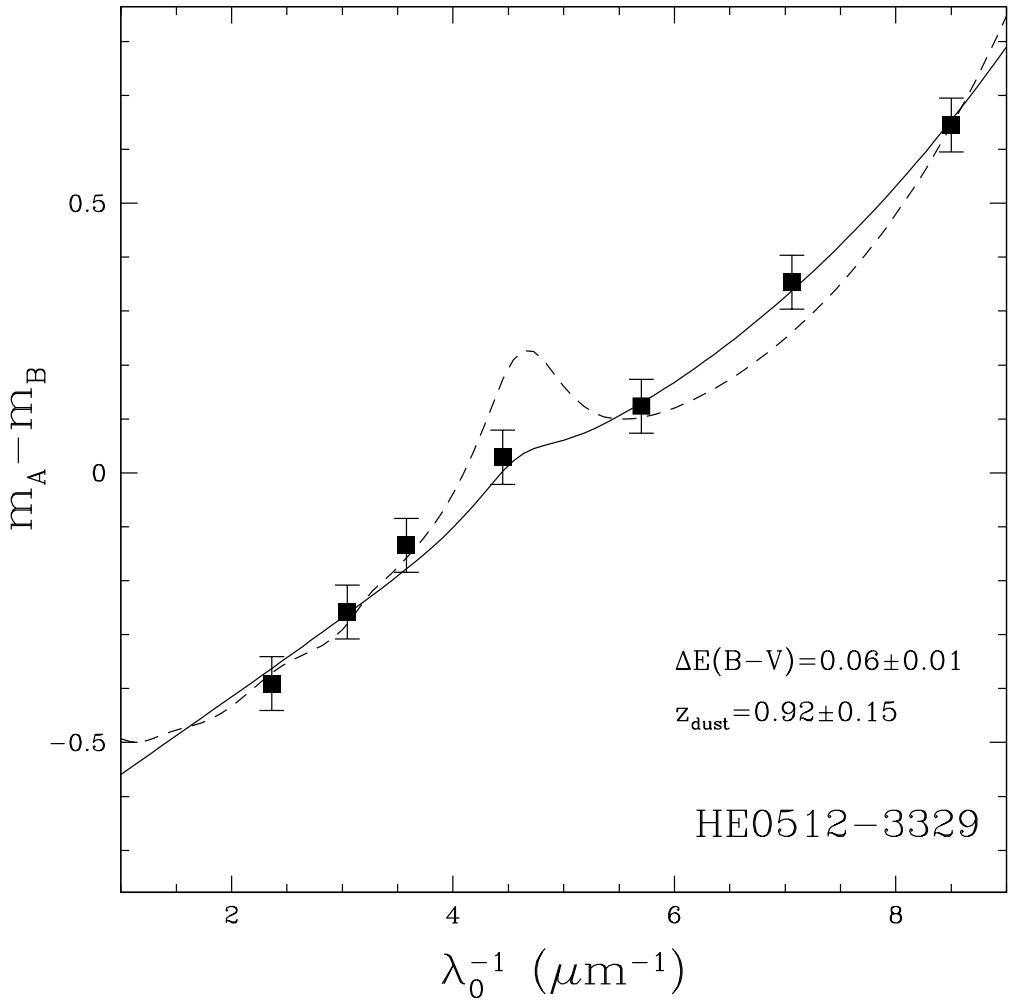


Fig. 3.— Magnitude differences as a function of the inverse of the lens rest-frame wavelength for the new HST observations (filled squares). The solid line shows the best fit FM extinction law allowing variations in the "stretch" of the bump and the dust redshift. The dashed line corresponds to the best fit for a Galactic CCM extinction law with $R(V) = 0.5$.

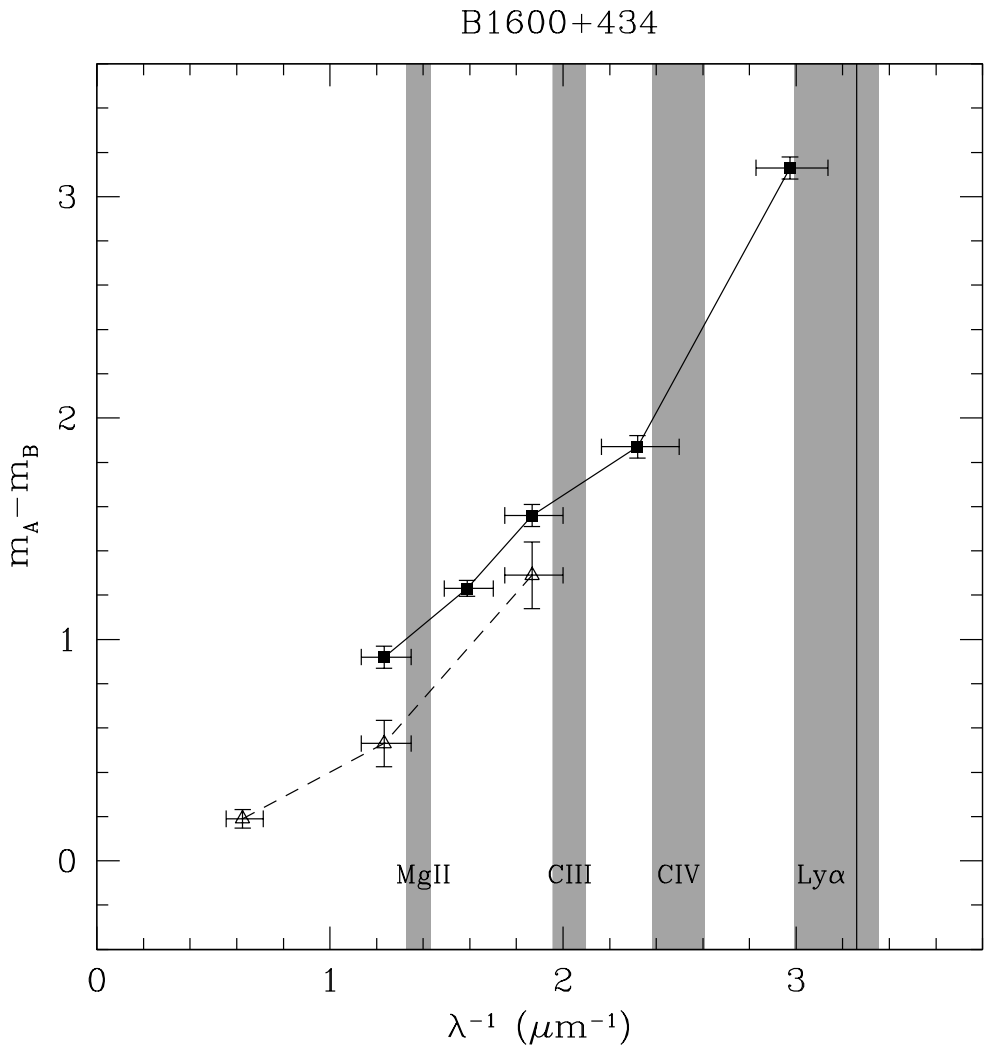


Fig. 4.— Magnitude differences of B 1600+434 as a function of the inverse of the observed wavelength for the new HST observations (filled squares) along with the previous CASTLES observations (open triangles). The format of the figure is the same as in Figure 2.

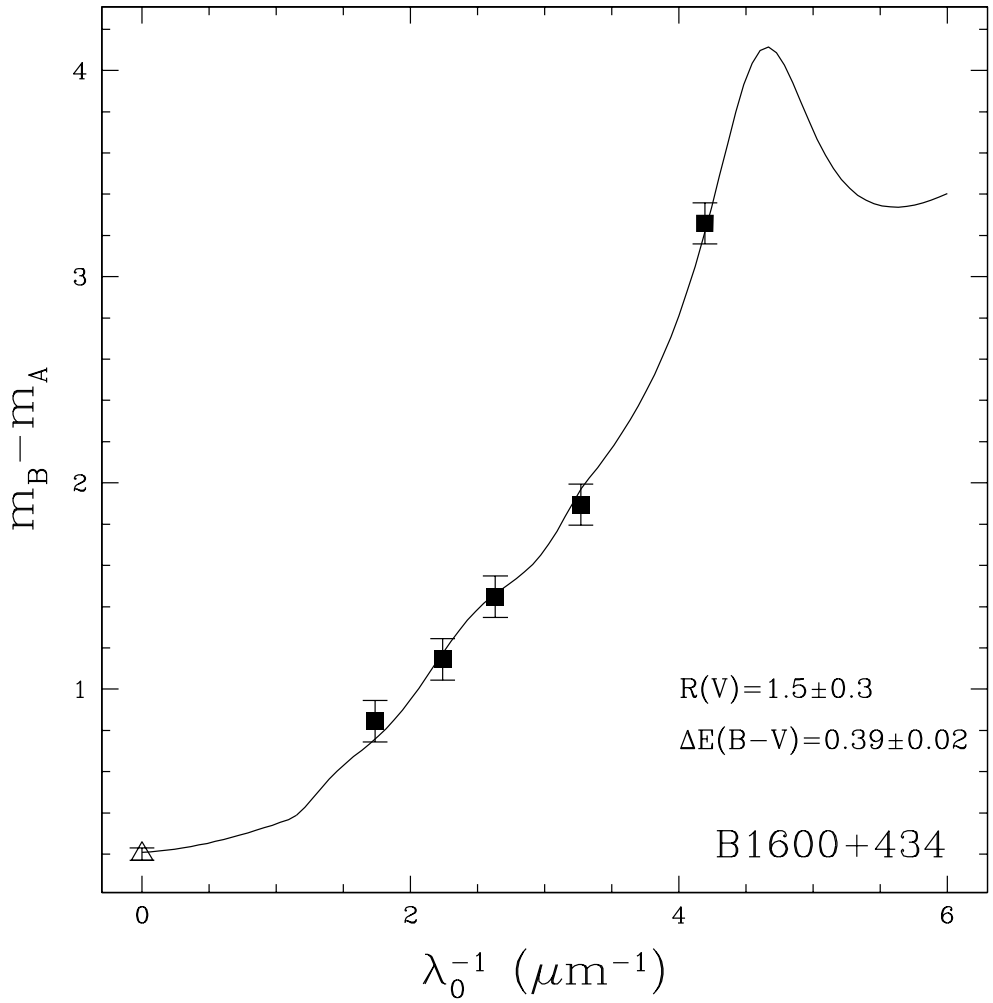


Fig. 5.— Magnitude differences as a function of the inverse of the lens rest-frame wavelength for the new HST observations (filled squares) and the 6 cm radio flux (open triangle) from Koopmans et al. (2000). The solid line shows the best fit for a CCM extinction law.

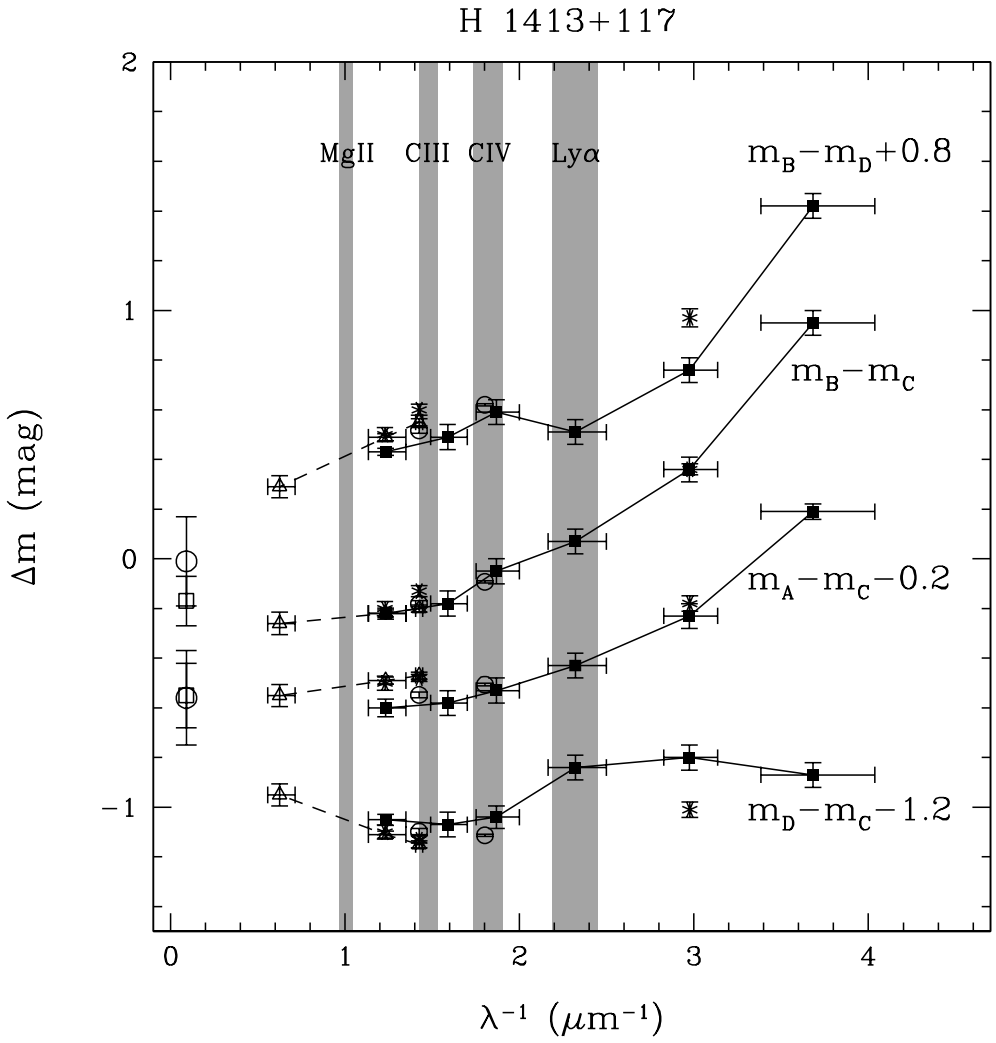


Fig. 6.— Magnitude differences of H 1413+117 as a function of the inverse of the observed wavelength for the new HST observations (filled squares) along with the previous CASTLES observations (open triangles) and the mid-infrared flux (large open symbols: squares or circles when de D image is present, see text) from MacLeod et al. (2009). We have also shown the results from Turnshek (1997) (asterisks) and Chae (2001) (open circles). In some cases these points are completely hidden by our new measurements. The format of the figure is the same as in Figure 2.

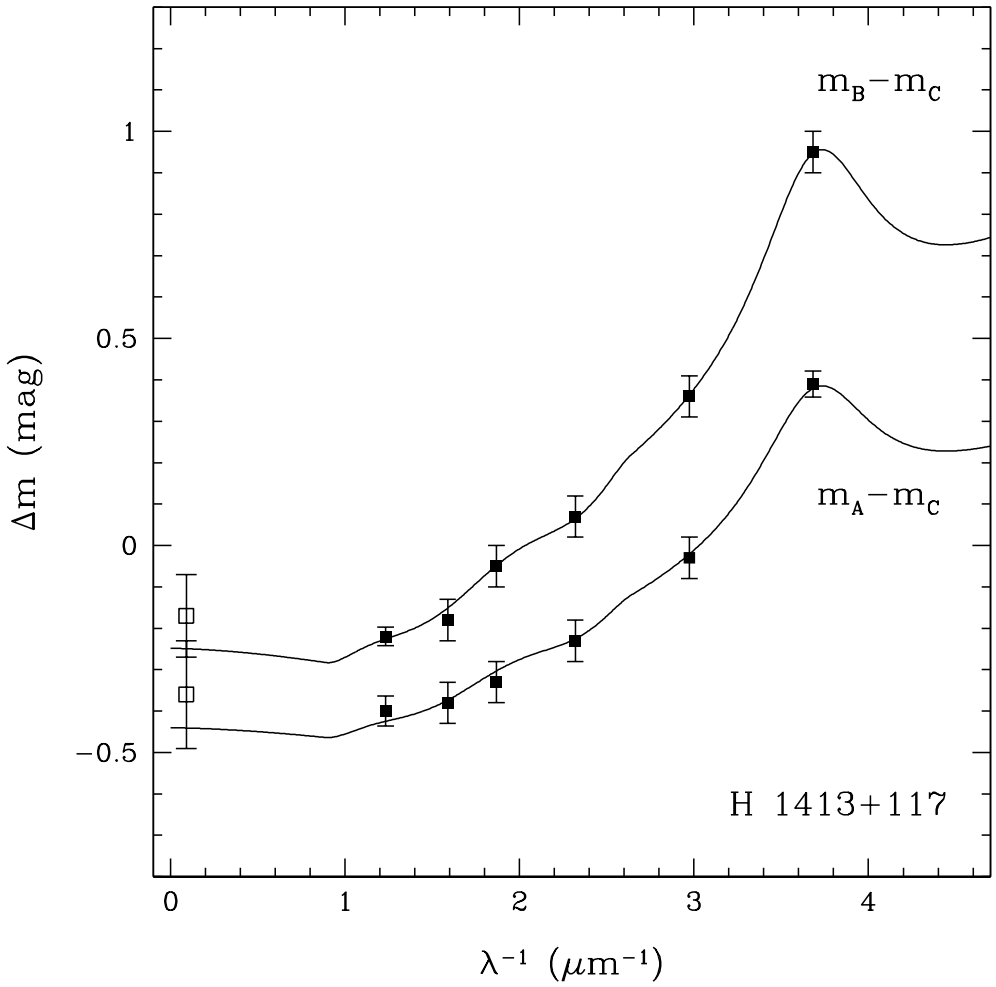


Fig. 7.— ACS/HRC and mid-infrared (MacLeod et al. 2009) magnitude differences $m_B - m_C$ and $m_A - m_C$, which are strongly indicative of extinction. As an example, the solid lines show fits with the same CCM extinction law for a fixed lens redshift $z_l = 0.25$. For the more probable, higher lens redshift, where the location of the 2175Å feature should be shifted to the left, successful fits require extinction laws without a strong 2175Å feature.

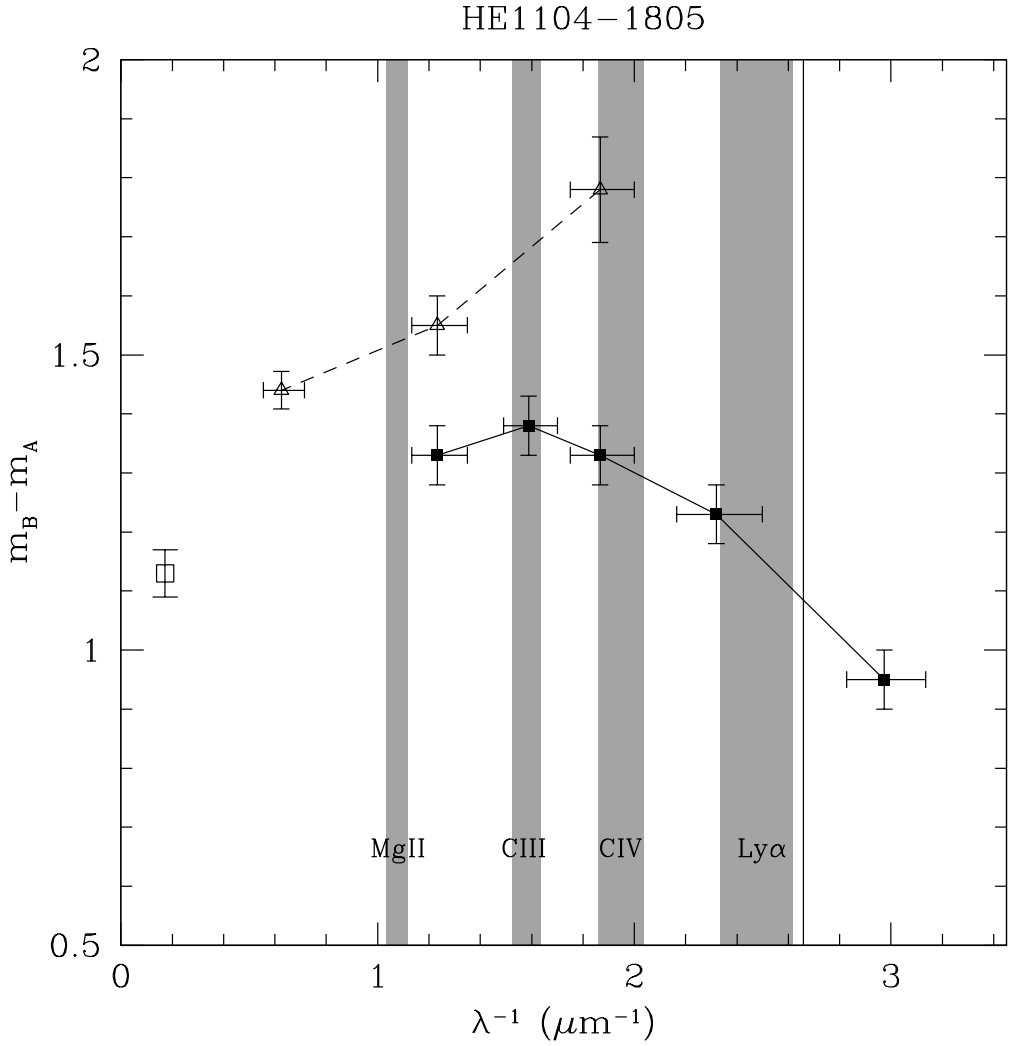


Fig. 8.— Magnitude differences of HE 1104−1805 as a function of the inverse of the observed wavelength for the new HST observations (filled squares) along with the previous CASTLES observations (open triangles) and the mid-IR observations (open square) from Poindexter et al. (2007). The format of the figure is the same as in Figure 2.

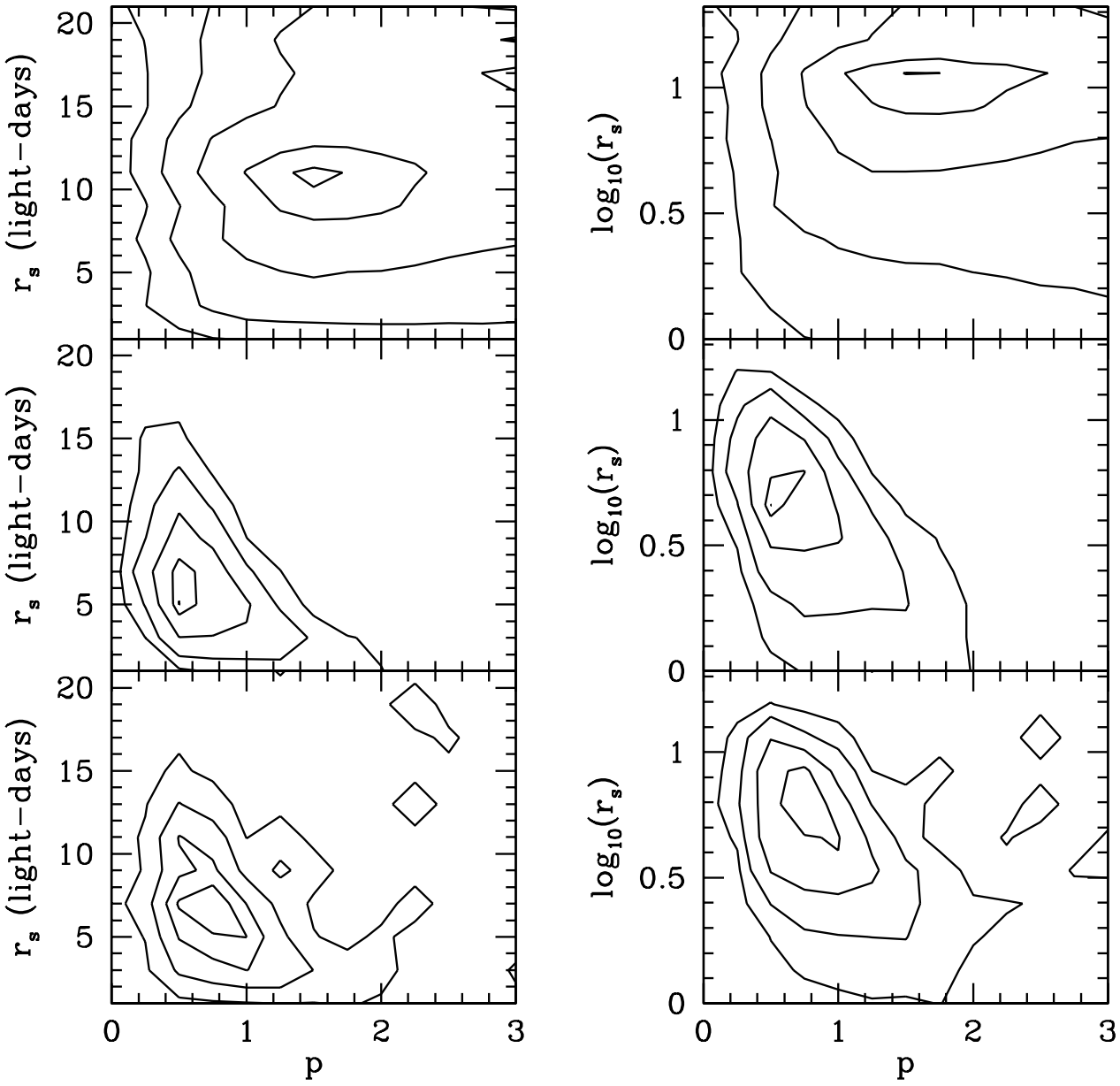


Fig. 9.— Probability distributions for the size of the quasar accretion disk r_s at an observed wavelength of 3363Å and the dependence of the size on wavelength, $r_s \propto \lambda^p$, assuming a linear (left) or logarithmic (right) prior for r_s, and using either the new HRC data (top), the older CASTLES data (middle) or the combined results (bottom). From the center, the contours are iso-probability density contours enclosing 15%, 47%, 68%, and 90% of the total probability, respectively.

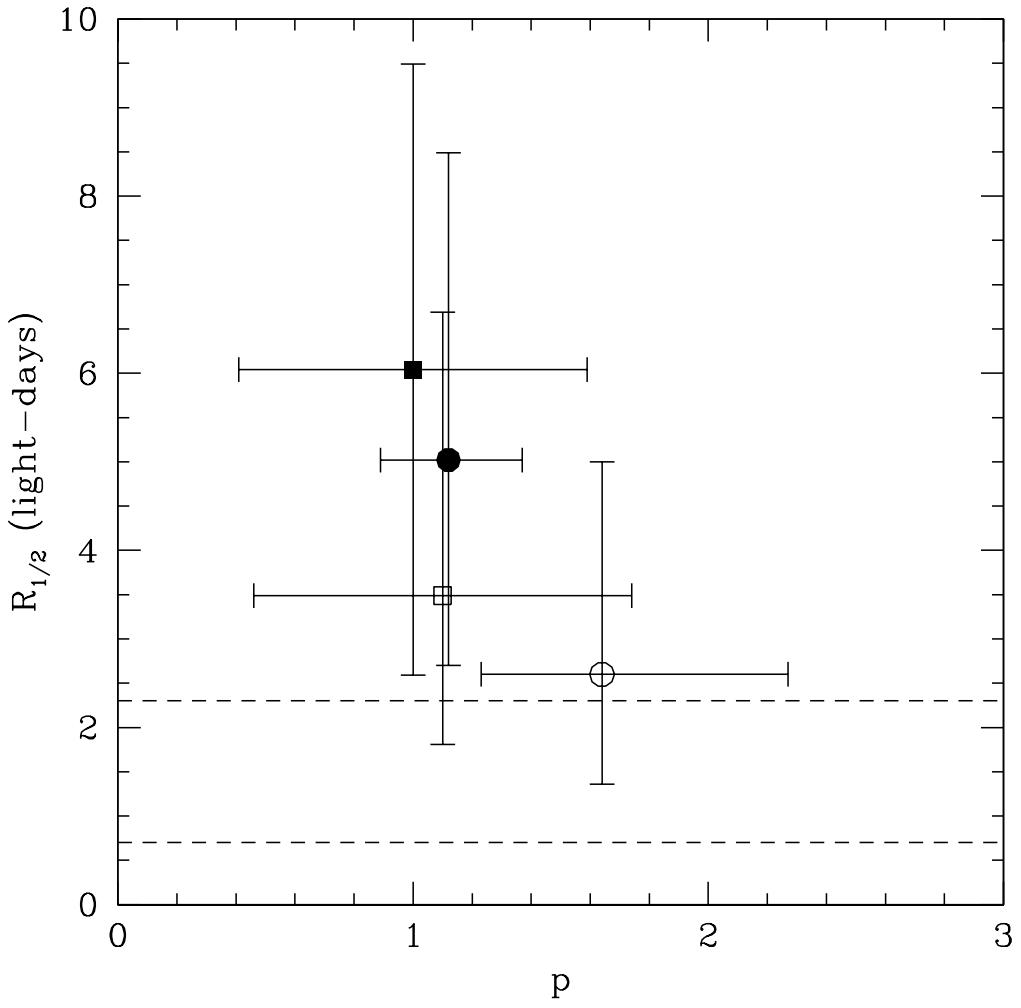


Fig. 10.— Comparisons of the half-light radii $R_{1/2}$ at $\lambda = 4311$Å for our combined single epoch models (squares) and the multi-band light curve analysis (circles) of Poindexter et al. (2008). Open (filled) symbols correspond to logarithmic (linear) priors on r_s. The dashed horizontal lines represent the size estimates inferred from the black-hole mass based on the thin disk theory (upper) or the observed I-band flux (lower) (see Poindexter et al. 2008). In this composition we have shifted the mean microlens mass to 0.3 $M_\odot$ (see text) in order to better compare to Poindexter et al. (2008).

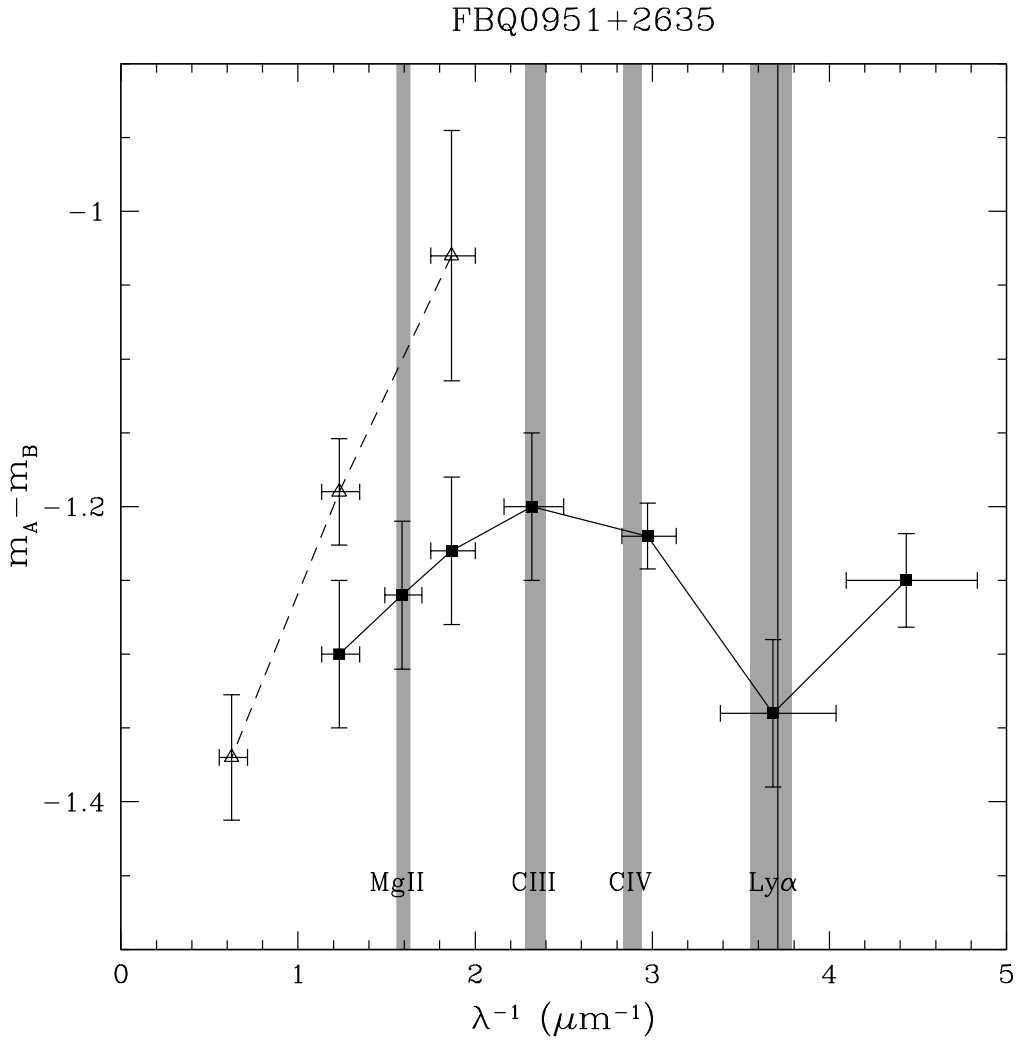


Fig. 11.— Magnitude differences of FBQ 0951+2635 as a function of the inverse of the observed wavelength for the new HST observations (filled squares) along with the previous CASTLES observations (open triangles). The format of the figure is the same as in Figure 2.

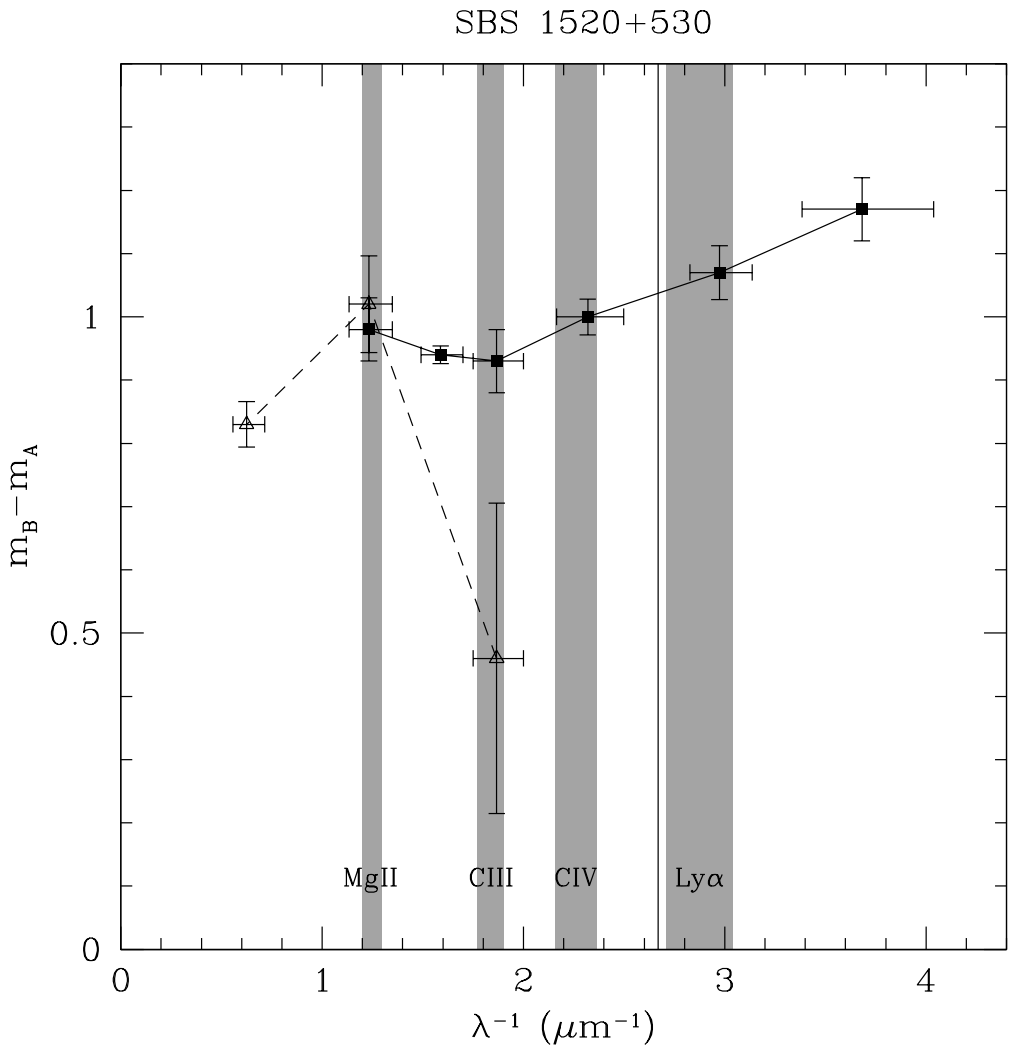


Fig. 12.— Magnitude differences of SBS 1520+530 as a function of the inverse of the observed wavelength for the new HST observations (filled squares) along with the previous CASTLES observations (open triangles). The format of the figure is the same as in Figure 2.

Table 1. Log of ACS/HRC Observations

TARGET	DATE-OBS (yyyy-mm-dd)	FILTER	EXP (sec)	No. of images
HE 0512−3329	2003-08-11	F220W	2136	2
	2003-08-11	F220W	3×712	2
	2003-08-11	F250W	408	2
	2003-08-11	F250W	3×136	2
	2003-08-11	F330W	129	2
	2003-08-11	F330W	3×43	2
	2003-08-11	F435W	36	2
	2003-08-11	F435W	3×12	2
	2003-08-11	F555W	27	2
	2003-08-11	F555W	3×9	2
	2003-08-11	F625W	24	2
	2003-08-11	F625W	3×8	2
	2003-08-11	F814W	6×3	2
	2003-08-11	F814W	18	2
	2003-08-11	F814W	3×6	2
FBQ 0951+2635	2003-10-06	F220W	368	2
	2003-10-06	F220W	2×184	2
	2003-10-06	F250W	116	2
	2003-10-06	F250W	2×58	2
	2003-10-06	F330W	50	2
	2003-10-06	F330W	25	2
	2003-10-07	F330W	25	2
	2003-10-06	F435W	16	2
	2003-10-06	F435W	8	2
	2003-10-07	F435W	8	2
	2003-10-06	F555W	12	2
	2003-10-06	F555W	6	2
	2003-10-07	F555W	6	2
	2003-10-06	F625W	8	2
	2003-10-06	F625W	4	2
	2003-10-07	F625W	4	2
	2003-10-06	F814W	8	2
	2003-10-06	F814W	4	2
	2003-10-07	F814W	4	2
HE 1104−1805	2003-11-05	F250W	2525	2
	2003-11-05	F250W	842	2
	2003-11-06	F250W	2×842	2
	2003-11-05	F330W	303	2
	2003-11-05	F330W	303	2
	2003-11-06	F330W	98	2
	2003-11-06	F330W	2×101	2
	2003-11-06	F435W	51	2
	2003-11-06	F435W	3×17	2
	2003-11-06	F555W	30	2
	2003-11-06	F555W	3×10	2
	2003-11-06	F625W	24	2
	2003-11-06	F625W	3×8	2
	2003-11-06	F814W	24	2
	2003-11-06	F814W	3×8	2
H 1413+117	2003-07-18	F330W	238	4
	2003-07-18	F330W	2×119	4
	2003-07-18	F435W	30	4
	2003-07-18	F435W	2×15	4
	2003-07-18	F555W	18	4
	2003-07-18	F555W	2×9	4
	2003-07-18	F625W	16	4

Table 1—Continued

TARGET	DATE-OBS (yyyy-mm-dd)	FILTER	EXP (sec)	No. of images
SBS 1520+530	2004-06-15	F250W	2484	2
	2004-06-15	F250W	3×828	2
	2004-06-15	F330W	561	2
	2004-06-15	F330W	3×187	2
	2004-06-15	F435W	141	2
	2004-06-15	F435W	3×47	2
	2004-06-15	F555W	90	2
	2004-06-15	F555W	3×30	2
	2004-06-15	F625W	68	2
	2004-06-15	F625W	3×26	2
	2004-06-15	F814W	62	2
	2004-06-15	F814W	3×24	2
B 1600+434	2003-08-17	F330W	4×1080	2
	2003-08-17	F435W	4×498	2
	2003-08-17	F555W	4×402	2
	2003-08-17	F625W	4×312	2
	2003-08-17	F814W	4×293	2

Table 2. CASTLES Photometry

Lens	Component	ΔR.A. (")	ΔDec (")	F555W†	F814W	F160W
HE 0512−3329	image A	0.182 ± 0.003	0.621 ± 0.003	18.15 ± 0.06	16.81 ± 0.08	15.81 ± 0.02
	image B	0	0	18.40 ± 0.09	17.28 ± 0.07	16.38 ± 0.03
	lens G	0.09 ± 0.07	0.37 ± 0.10	22.1 ± 0.6	20.9 ± 0.7	19.1 ± 0.8
FBQ 0951+2635	image A	0	0	17.29 ± 0.06	16.70 ± 0.03	15.62 ± 0.03
	image B	0.900 ± 0.003	-0.635 ± 0.003	18.32 ± 0.06	17.89 ± 0.02	16.99 ± 0.03
	lens G	0.760 ± 0.003	-0.455 ± 0.003	21.02 ± 0.04	19.67 ± 0.03	17.86 ± 0.14
HE 1104−1805	image A	0	0	16.92 ± 0.06	16.40 ± 0.03	15.91 ± 0.01
	image B	2.901 ± 0.003	-1.332 ± 0.003	18.70 ± 0.08	17.95 ± 0.04	17.35 ± 0.03
	lens G	0.965 ± 0.003	-0.500 ± 0.003	23.26 ± 0.30	20.01 ± 0.10	17.52 ± 0.09
H 1413+117	image A	0	0	18.00 ± 0.01	17.77 ± 0.01	15.83 ± 0.04
	image B	0.744 ± 0.003	0.168 ± 0.003	18.07 ± 0.01	17.84 ± 0.01	15.92 ± 0.03
	image C	-0.492 ± 0.003	0.713 ± 0.003	18.27 ± 0.01	18.06 ± 0.01	16.18 ± 0.02
	image D	0.354 ± 0.003	1.040 ± 0.003	18.32 ± 0.01	18.15 ± 0.01	16.43 ± 0.03
	lens G	0.142 ± 0.003	0.561 ± 0.003	–	–	18.61 ± 0.03
SBS 1520+530	image A	0	0	18.83 ± 0.05	17.97 ± 0.03	17.58 ± 0.02
	image B	1.429 ± 0.003	-0.652 ± 0.003	19.29 ± 0.24	18.99 ± 0.07	18.41 ± 0.03
	lens G	1.141 ± 0.003	-0.395 ± 0.003	23.40 ± 2.00	20.16 ± 0.11	18.22 ± 0.05
B 1600+434	image A	0	0	23.61 ± 0.12	21.92 ± 0.10	20.66 ± 0.03
	image B	-0.720 ± 0.003	1.183 ± 0.004	22.32 ± 0.09	21.39 ± 0.03	20.47 ± 0.03
	lens G	-0.110 ± 0.003	0.369 ± 0.004	–	20.78 ± 0.06	18.30 ± 0.13

Note. — † For the system H 1413+117 it corresponds to the filter F702W

Table 3. ACS/HRC Photometry

Lens	Image	F220W	F250W	F330W	F435W	F555W	F625W	F814W
HE 0512−3329	A	18.96±0.11	18.07±0.23	17.67±0.13	18.67±0.03	18.10±0.05	17.60±0.05	16.98±0.03
	B	18.33±0.04	17.74±0.02	17.55±0.03	18.66±0.02	18.25±0.04	17.88±0.03	17.36±0.03
FBQ 0951+2635	A	16.72±0.01	16.36±0.03	16.60±0.02	17.80±0.04	17.48±0.03	17.14±0.03	16.82±0.03
	B	17.97±0.03	17.70±0.08	17.82±0.01	19.00±0.08	18.71±0.04	18.40±0.10	18.12±0.05
HE 1104−1805	A	···	···	17.25±0.05	17.81±0.07	17.57±0.10	17.33±0.06	16.85±0.05
	B	···	···	18.20±0.09	19.04±0.12	18.90±0.11	18.71±0.12	18.18±0.07
H 1413+117	A	···	20.84±0.03	18.97±0.07	18.61±0.06	18.20±0.09	17.75±0.02	17.70±0.03
	B	···	21.40±0.12	19.36±0.08	18.91±0.12	18.48±0.07	17.95±0.05	17.88±0.01
	C	···	20.45±0.01	19.00±0.01	18.84±0.03	18.53±0.04	18.13±0.05	18.10±0.02
	D	···	20.78±0.10	19.40±0.06	19.20±0.09	18.69±0.02	18.26±0.04	18.25±0.01
SBS 1520+530	A	···	18.23±0.07	17.86±0.03	18.94±0.02	18.73±0.03	18.52±0.01	18.12±0.04
	B	···	19.40±0.10	18.93±0.03	19.94±0.02	19.66±0.04	19.46±0.01	19.10±0.04
B 1600+434	A	···	···	25.68±0.47	25.36±0.11	24.63±0.10	23.67±0.02	22.68±0.03
	B	···	···	22.55±0.17	23.49±0.25	23.07±0.11	22.44±0.03	21.76±0.06

Table 4. Quasar Accretion Disk Measurements for HE 1104−1805

	ACS	CASTLES	ACS x CASTLES
		Logarithmic prior	
r_s (light-days)	6^{+8}_{-4}	4^{+4}_{-2}	4^{+4}_{-2}
p	1.8±0.8	1.0±0.7	1.1±0.6
		Linear prior	
r_s (light-days)	12±6	7±4	7±4
p	1.8±0.8	0.9±0.6	1.0±0.6

Note. — r_s is the size of the quasar accretion disk modeled as a Gaussian ($I(R) \propto \exp(-R^2/2r_s^2)$) at the observed wavelength $\lambda = 3363\,\text{Å}$ and p is the power law of the size variation with wavelength ($r_s(\lambda) \propto \lambda^p$).